LA-UR-19-27140

Approved for public release; distribution is unlimited.

Title:	Observations of Poorly-Known Features of the 239Pu and 235U Prompt Fission Neutron Spectra
Author(s):	Kelly, Keegan John; Gomez, Jaime A.; O'Donnell, John M.; Devlin, Matthew James; Haight, Robert Cameron; Taddeucci, Terry Nicholas; Mosby, Shea Morgan; Lee, Hye Young; Neudecker, Denise; Kawano, Toshihiko; Lovell, Amy Elizabeth; Talou, Patrick; White, Morgan Curtis; Wu, Ching-Yen; Henderson, Roger Alan; Henderson, Jack; Buckner, Matthew Quinn
Intended for:	Nuclear Data 2019, 2019-05-19/2019-05-24 (Beijing, China)
Issued:	2019-07-24

Observations of Poorly-Known Features of the ^{239}Pu and ^{235}U Prompt Fission Neutron Spectra

Keegan J. Kelly[1,*], *Jaime A.* Gomez[1], *John M.* O'Donnell[1], *Matthew* Devlin[1], *Robert C.* Haight[1], *Terry N.* Taddeucci[1], *Shea M.* Mosby[1], *Hye Young* Lee[1], *Denise* Neudecker[1], *Toshihiko* Kawano[1], *Amy E.* Lovell[1], *Patrick* Talou[1], *Morgan C.* White[1], *Ching-Yen* Wu[2], *Roger A.* Henderson[2], *Jack* Henderson[2], and *Matthew Q.* Buckner[2]

[1]Los Alamos National Laboratory, Los Alamos, NM 87545, USA
[2]Lawrence Livermore National Laboratory, Livermore, CA 94550, USA

Abstract. Prompt fission neutron spectrum (PFNS) evaluations use available nuclear data to predict the PFNS across a wide range of incident and outgoing neutron energies. However, these data are sparse, inconsistent, and incomplete with respect to the desired energy coverage. As such, evaluations sometimes predict features of the PFNS, such those relating to multi-chance fission and pre-equilibrium pre-fission neutron emission, without any experimental verification. The Chi-Nu experiment at Los Alamos National Laboratory has recently obtained high-precision results for the ^{239}Pu and ^{235}U PFNS which, for the first time in most cases, have shed light on multi-chance fission and pre-equilibrium contributions to the observed fission neutron spectrum. In addition to providing the first experimental data on some of these fission properties, the angular coverage of the Chi-Nu experiment allowed for the extraction of angular distributions of pre-equilibrium pre-fission neutrons. PFNS results of multi-chance fission and pre-equilibrium pre-fission neutron emission are discussed in this proceedings in terms of the observed neutron spectrum and the average PFNS energies.

1 Introduction

Knowledge of the energy spectrum of neutrons emitted promptly following neutron-induced fission, i.e., the prompt fission neutron spectrum (PFNS), is essential for any system relating to neutron-driven chain reactions, but PFNS measurements even on the major actinides ^{235}U and ^{239}Pu are sparse and inconsistent [1–3]. Furthermore, there has only been one previous white-source PFNS measurement (see the ^{239}Pu PFNS measurement of Ref. [4, 5]), but these results have been shown to contain a systematic bias requiring an uncertain correction [6]. The Chi-Nu experiment at the Los Alamos Neutron Science Center is designed to measure the PFNS of major actinides over the incident neutron energy range of E_n^{inc} = 1–20 MeV and outgoing neutron energies from E_n^{out} = 0.01–10 MeV [7–10]. Neither the Chi-Nu experiment nor the PFNS results for $E_n^{inc} \leq 5$ MeV will be described here because these are described by M. Devlin in these proceedings. Here we will instead focus on observations of poorly-known features of the PFNS of ^{235}U and ^{239}Pu for $E_n^{inc} > 5$ MeV.

A common simplified picture of neutron-induced fission on, for example, ^{239}Pu is that the excited ^{240}Pu daughter nucleus fissions into, typically, two fragments that then emit neutrons and γ rays. This type of fission is referred to as first-chance fission and is the most likely type of fission for lower incident neutron energies. However, if enough excess energy exists for a neutron to be emitted prior to fission, then a ^{239}Pu nucleus can fission instead of ^{240}Pu,
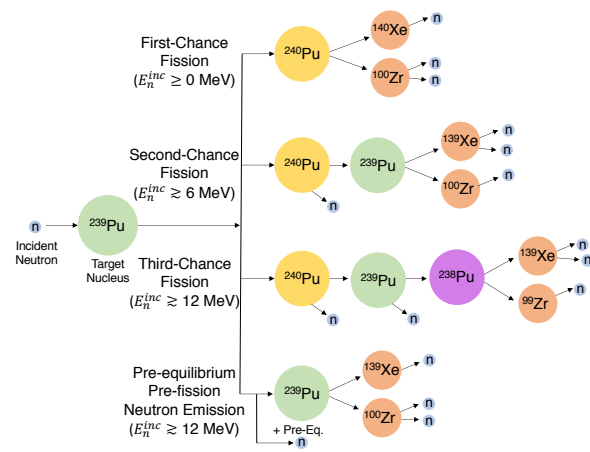

Figure 1. An illustration of the paths to various fissioning nuclei for incident neutron energies below 20 MeV is shown here for a ^{239}Pu target nucleus. This is a reproduction of Fig. 1 of Ref. [11]. The evolution of the PFNS with increasing incident neutron energy is the convolution of these various possible fission paths, each of which may produce different features in the measured neutron spectrum in coincidence with fission.

and similarly a ^{238}Pu nucleus can fission for even higher incident neutron energies. These processes are referred to as second- and third-chance fission, and the corresponding incident neutron-energy thresholds are typically $E_n^{inc} \approx 6$
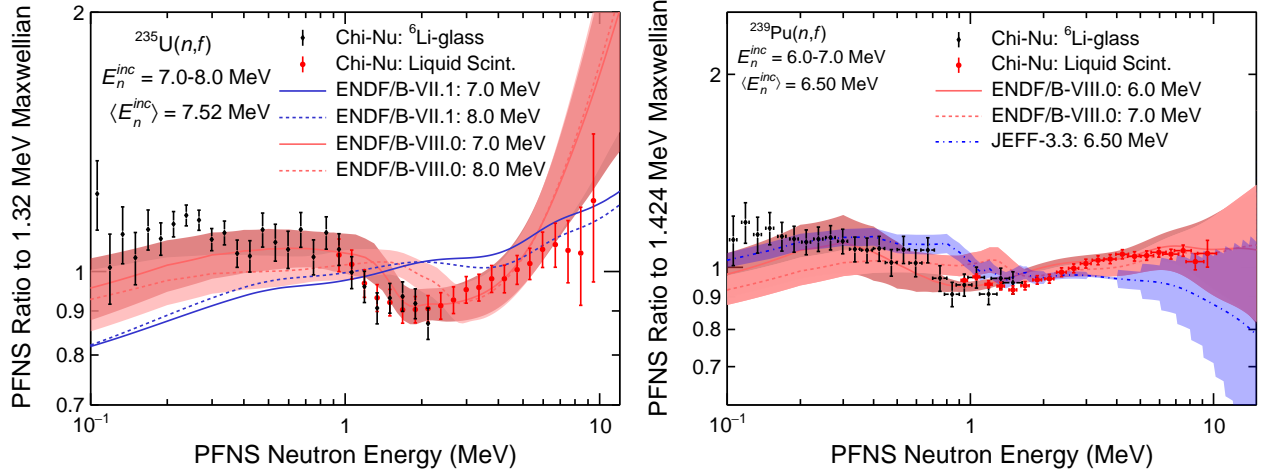
Figure 2. Second-chance fission PFNS features observed by the Chi-Nu experiment for neutron-induced fission of ^{235}U (left) and ^{239}Pu (right) are shown here. The experimental incident neutron-energy ranges are shown in each plot. The bands and trends correspond to evaluations at relevant incident neutron energies [12–14].

MeV and $E_n^{inc} \approx 12$ MeV, respectively. Finally, beginning at $E_n^{inc} \approx 12$ MeV the reaction can occur by the emission of a pre-equilibrium neutron that leaves the residual nucleus in an excited state, which can then subsequently undergo fission if the excitation energy is high enough. A schematic illustration of these types of fission is shown in Fig. 1. The features that these different fission processes create in the PFNS of ^{235}U and ^{239}Pu are discussed in Sec. 2 and the impacts on the average energy of the PFNS at each incident neutron energy are shown in Sec. 3.

2 Multi-Chance and Pre-Equilibrium PFNS Features

Measurements of the PFNS are commonly tagged on a fission signal, but strictly speaking, neutrons measured in coincidence with this fission signal are not guaranteed to be "prompt fission neutrons", i.e., neutrons emitted promptly following fission. The extremely short timescales associated with nuclear fission make it experimentally impossible to separate neutrons emitted after fission (true postfission, PFNS neutrons) from those emitted prior to fission (pre-fission neutrons). For this reason, all experimental PFNS measurements contain pre-fission neutrons from all available multi-chance fission and pre-equilibrium neutron contributions in addition to post-fission neutrons. These different contributions create distinct structures in the observed neutron spectrum, and even unique angular distributions associated with the different spectral contributions.

The left panel of Figs. 2 and 3 show PFNS structures at $E_n^{out} \approx 0.1$–1.0 MeV that appear near the onset of second- and third-chance fission of ^{235}U, and the right panel of Figs. 2 and 3 show the same features for ^{239}Pu. Multi-chance fission typically manifests in the PFNS as a distribution of counts that peaks at roughly $E_{inc} - E_b$, where E_b is the fission barrier height for the chance of fission under study. Therefore, observations of these PFNS features provide valuable information to evaluators on these fission

barrier heights. However, note that third-chance fission does not appear to the level predicted by evaluations in the ^{239}Pu PFNS, shown in the right panel of Fig. 3. The ENDF/B-VII.1 [14] and ENDF/B-VIII.0 [13] evaluations are shown in the left panel of Figs. 2 and 3 to highlight the improvements made between these two evaluations, which were in part due to the inclusion of low outgoing-energy PFNS data from Chi-Nu above $E_n^{inc} = 5$ MeV [9]. The ENDF/B-VIII.0 and JEFF-3.3 [12] evaluations are shown in the right panel of Figs. 2 and 3 to shown the differences between these two recent evaluations and the Chi-Nu results. The average PFNS energy plots shown in Sec. 3 add an additional interesting point to this comparison.

Also shown in Fig. 3 are the measured PFNS features corresponding to pre-equilibrium neutron emission at $E_n^{out} \approx 6$–9 MeV. This feature again corresponds to a distribution of counts, but this distribution is sharply peaked at $E_{inc} - E_b$ and corresponds to neutrons that were emitted prior to establishing nuclear equilibrium, as opposed to pre-fission neutrons emitted before second- and third-chance fission that are emitted after establishing equilibrium. Given the clarity with which the pre-equilibrium structure was observed in the ^{239}Pu PFNS, it was possible to separate counts within the peak of the pre-equilibrium neutron distribution corresponding solely to the pre-equilibrium process from the underlying (predominantly) post-fission neutron spectrum. These results were described in Ref. [11], where it was also shown that these counts appear to have an angular distribution consistent with a pure inelastic scattering reaction, providing experimental support to the theory that there is little-to-no correlation between the fission axis and the pre-equilibrium neutron angular distribution.

3 Average PFNS Energies

While the fine details of the PFNS itself are important, the average PFNS energy, $\langle E \rangle$, is informative as well and the
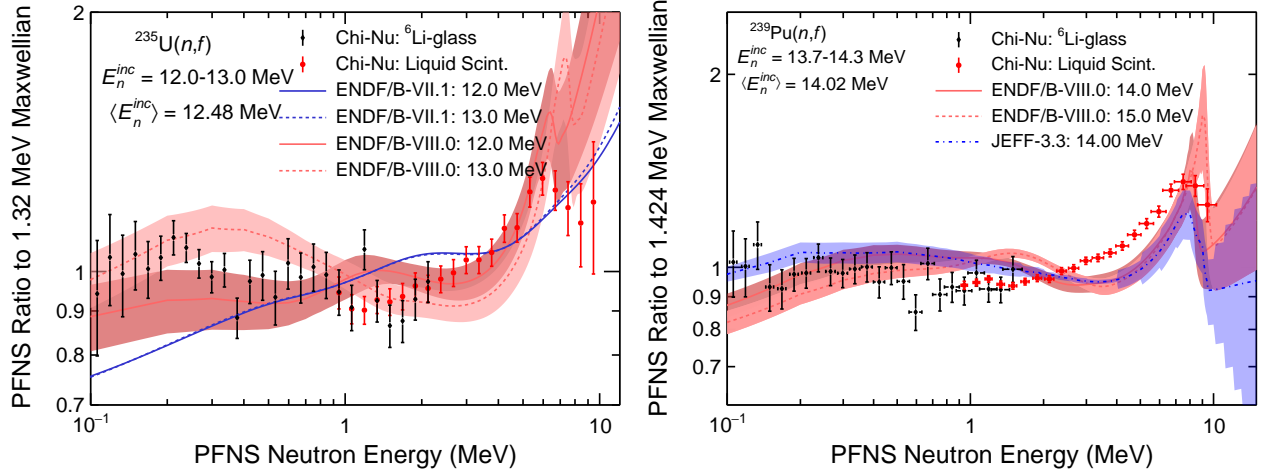
Figure 3. Third-chance fission and pre-equilibrium PFNS features observed by the Chi-Nu experiment for neutron-induced fission of ^{235}U (left) and ^{239}Pu (right) are shown here. The bands and trends correspond to evaluations at relevant incident neutron energies [12–14].
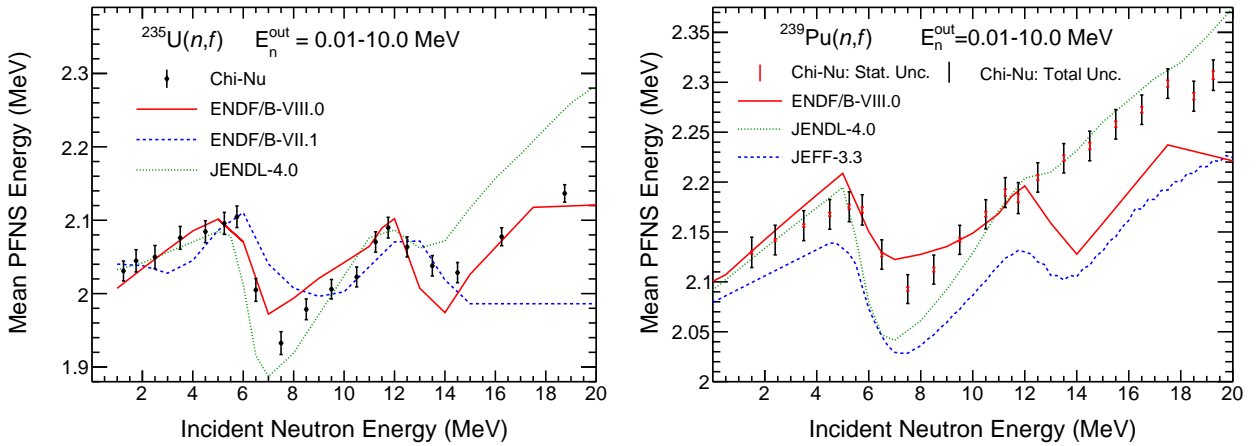

Figure 4. The trend of the average PFNS energy, $\langle E \rangle$, as a function E_n^{inc} is shown here for ^{235}U and ^{239}Pu in the left and right panels, respectively. Relevant evaluations are plotted as well for comparison. The ^{239}Pu $\langle E \rangle$ uncertainties are also subdivided into statistical and systematic components to demonstrate the importance of identifying and quantifying all possible sources of systematic uncertainty. The ^{235}U only has a subset of the total known systematic uncertainty applied for the data in this proceedings.

features of the PFNS described in Sec. 2 are also directly reflected in $\langle E \rangle$. The left and right panels of Fig. 4 show the $\langle E \rangle$ trends as a function of E_n^{inc} measured for ^{235}U and ^{239}Pu, respectively, compared to recent nuclear data evaluations. Since multi-chance fission creates an excess at low-energies in the PFNS, there should be a corresponding drop in $\langle E \rangle$ at $E_n^{inc} \approx 6$ and 12 MeV. Both of these drops are observed for ^{235}U, but the third-chance fission PFNS contribution appears to be much weaker than predicted by evaluations in ^{239}Pu. This conclusion is supported by the spectra shown in the right panel of Fig. 2.

An improvement on PFNS measurements to be made with Chi-Nu PFNS results that will be published in the future [15] is the correlation of the measured PFNS data points across both outgoing and incident neutron energy, which can then yield insight into how reliable the *shape* of the $\langle E \rangle$ trend is, as opposed to the absolute values. This in-

formation will add further insight to the comparison of, for example, the Chi-Nu ^{239}Pu PFNS $\langle E \rangle$ trend to that of the JEFF-3.3 [12] evaluation, which appear to have very similar shapes for the majority of the plotted incident neutron-energy range despite the ~100 keV offset between them and despite the fact that Chi-Nu PFNS shapes tend to agree better with ENDF/B-VIII.0 than with JEFF-3.3. This will be discussed further in future publications.

4 Conclusions

The evolution of the PFNS from $E_n^{inc} = 1$–20 MeV needs to be known for understanding the fission process and for applications, though at present it is not well known experimentally or theoretically. Existing data are lacking in that few experiments measure the actinide PFNS at multiple incident neutron energies, and the few previous white-

source PFNS measurements of ^{239}Pu resulted in discrepancies. The Chi-Nu experiment is providing detailed information on the PFNS of major actinides across multiple orders of magnitude of outgoing neutron energy for incident neutron energies from 1–20 MeV. The observations described in this proceedings show the current state of the Chi-Nu measurements of the ^{235}U and ^{239}Pu PFNS, with a focus on features of the PFNS that are either poorly-known or have never been measured before.

In addition to providing state-of-the-art PFNS experimental results, the analysis of data from the Chi-Nu experiment includes an unprecedented level of attention to systematic uncertainties and biases in neutron detection experiments, along with associated covariances across all measured outgoing energies and across multiple neutron detector arrays [16]. Future Chi-Nu results will also include covariances between all incident neutron energies, thereby creating a single, well-described, correlated PFNS result for the majority of the PFNS incident and outgoing neutron energy range of interest. This level of information has never been obtained for any previous PFNS experiment, and will allow for separate assessments of the PFNS evolution as a function of incident neutron energy in terms of both shape and magnitude. Finally, the Chi-Nu team also intends to provide detailed documentation on every aspect of the experiment and of the analysis. This documentation will allow future experimenters and evaluators to modify Chi-Nu results as new information and advances in nuclear physics are made, thereby ensuring that Chi-Nu data never become obsolete.

References

[1] R. Capote, Y.J. Chen, F.J. Hambsch, N.V. Kornilov, J.P. Lestone et al., Nucl. Data Sheets **131**, 1 (2016)

[2] D. Neudecker, T.N. Taddeucci, R.C. Haight, H.Y. Lee, M.C. White et al., Nucl. Data Sheets **131**, 289 (2016)

[3] D. Neudecker, P. Talou, T. Kawano, A. Kahler, M. White et al., Nucl. Data Sheets **148**, 293 (2018)

[4] S. Noda, R.C. Haight, R.O. Nelson, M. Devlin, J.M. O'Donnell et al., Phys. Rev. C **83**, 034604 (2011)

[5] A. Chatillon, G. Bélier, T. Granier, B. Laurent, B. Morillon et al., Phys. Rev. C **89**, 014611 (2014)

[6] T. Granier, Phys. Proc. **64**, 183 (2015)

[7] R.C. Haight, C.Y. Wu, H.Y. Lee, T.N. Taddeucci, B.A. Perdue et al., Nucl. Data Sheets **123**, 130 (2015)

[8] T.N. Taddeucci, R.C. Haight, H.Y. Lee, D. Neudecker, J.M. O'Donnell et al., Nucl. Data Sheets **123**, 135 (2015)

[9] M. Devlin, J.A. Gomez, K.J. Kelly, R.C. Haight, J.M. O'Donnell et al., Nucl. Data Sheets **148**, 322 (2018)

[10] K.J. Kelly, J.A. Gomez, J.M. O'Donnell, M. Devlin, R.C. Haight et al., Proceedings of the 20th Topical Meeting of the Radiation Protection and Shielding Division (2018)

[11] K.J. Kelly, T. Kawano, J.M. O'Donnell, J.A. Gomez, M. Devlin et al., Phys. Rev. Lett. **122**, 072503 (2019)

[12] *The Joint Evaluated Fission and Fusion File (JEFF), Version 3.3*, https://www.oecd-nea.org/dbdata/jeff/jeff33/index.html

[13] D.A. Brown, M.B. Chadwick, R. Capote, A.C. Kahler, A. Trkov et al., Nucl. Data Sheets **148**, 1 (2018)

[14] M.B. Chadwick, M. Herman, P. Oblŏzinský, M.E. Dunn, Y. Danon et al., Nucl. Data Sheets **112**, 2887 (2011)

[15] K.J. Kelly, M. Devlin, J.A. Gomez, J.M. O'Donnell, R.C. Haight et al., Phys. Rev. C **In Preparation** (2019)

[16] K.J. Kelly, J.M. O'Donnell, M. Devlin, D. Neudecker, J.A. Gomez, Nucl. Instrum. and Methods A **Under Review** (2019)